Ultrafast phase transitions and lattice dynamics probed using laser-produced x-ray pulses

2004 J. Phys.: Condens. Matter 16 R1517

(http://iopscience.iop.org/0953-8984/16/49/R04)

INSTITUTE OF PHYSICS PUBLISHING JOURNAL OF PHYSICS: CONDENSED MATTER

J. Phys.: Condens. Matter **16** (2004) R1517–R1536 PII: S0953-8984(04)60719-3

TOPICAL REVIEW

Ultrafast phase transitions and lattice dynamics probed using laser-produced x-ray pulses

Klaus Sokolowski-Tinten[1] **and Dietrich von der Linde**[2]

[1] Institut für Optik und Quantenelektronik, Friedrich-Schiller-Universität Jena, Max-Wien-Platz 1, 07743 Jena, Germany
[2] Institut für Laser- und Plasmaphysik, Universität Duisburg-Esssen, 45117 Essen, Germany

Received 31 July 2004, in final form 14 September 2004
Published 26 November 2004
Online at stacks.iop.org/JPhysCM/16/R1517
doi:10.1088/0953-8984/16/49/R04

Abstract

When intense femtosecond laser pulses are focused on solid targets short-lived microplasmas are formed which emit bursts of x-rays with kilovolt photon energies. Under the proper conditions x-ray pulses as short as a few hundred femtoseconds can be produced. These x-ray pulses enable ultrafast x-ray spectroscopy using pump–probe schemes where the x-ray pulses serve as probe pulses. This article describes time-resolved x-ray diffraction experiments which reveal changes in the atomic structure with a time resolution of a few hundred femtoseconds. In particular, we have studied solid-to-liquid phase transitions in semiconductors induced by femtosecond photoexcitation and the accompanying thermoacoustic phenomena. We were able to monitor the changes in the atomic position underlying a coherent optical phonon mode. These and a number of other lattice dynamics experiments discussed here demonstrate the feasibility and usefulness of ultrafast time-resolved x-ray diffraction. Future applications in many other fields of science can be foreseen.

Contents

1. Introduction

Knowledge of the atomic structure of matter is of fundamental importance in science. The discovery of important structural information has often led to the creation of a new field. A good example is the foundation of modern solid state physics following the discovery by von Laue of x-ray diffraction from crystal lattices which enabled him to show that the crystal structure could be obtained by measuring x-ray diffraction patterns [1]. A second example is the discovery of the double helix structure of DNA by Watson and Crick [2]. This finding may be regarded as the beginning of modern molecular biology and of genetic engineering.

Diffraction experiments, in particular x-ray diffraction ones, have been very important tools in structural science. So far, however, diffraction methods have essentially provided a view of the static structure. Although changes in the structure of matter may be measured using time-resolved methods, it has been impossible to directly observe the atomic motions leading to a structural change. In a chemical reaction, for example, the structure of the starting material could be measured, and that of the end product, but it was not possible to follow the detailed steps of the elementary reactions on an atomic level.

The reason is, of course, that atoms move very fast and changes to an atomic configuration occur very rapidly. The typical timescale for the change in atomic configurations is the femtosecond timescale, roughly speaking from 10^{-12} down to 10^{-14} s. These times are comparable with the duration of the cycles of molecular vibrations. Although femtosecond laser pulses have been available for quite some time and have enabled optical measurements with femtosecond time resolution, these optical techniques cannot directly provide a view of the atomic structure. This is because the wavelength of light is so much larger than the sizes and distances of the atoms in molecules and crystals. Information on structural changes could only be derived indirectly from the secondary effects that structural changes have on the optical properties.

This situation is now changing rapidly. Some x-ray sources that produce flashes only a few hundred femtoseconds in duration are already available and new kinds of x-ray sources are being developed which will provide very powerful x-ray pulses of one hundred femtoseconds or less [3]. The important feature of these new sources of ultrashort x-ray pulses is that they enable physical experiments *combining femtosecond time resolution and atomic scale spatial resolution*. The vision of scientists being able to take snapshots of the atomic structure will therefore become reality.

2. Femtosecond laser-produced plasmas as x-ray sources

In the past decade impressive progress has been made in the generation of ultrashort laser pulses of extremely high peak intensity [4]. These developments have made it possible to carry out new kinds of experiments [5] such as the acceleration of charged particles by strong laser fields and the triggering of nuclear reactions from laser pulses. They have also provided new methods for the generation of x-rays [6], in particular, very short x-ray pulses [7].

During the interaction with a strong laser pulse matter becomes fully ionized and is turned into a plasma. The kinetic energy of the plasma electrons depends on the laser intensity and can reach tens or hundreds of electron volts at readily attainable laser intensity. The interaction of these energetic electrons with the material gives rise to bremsstrahlung and characteristic x-ray line radiation, in very much the same way that x-rays are generated in an ordinary x-ray tube. However, the fundamental difference is the duration of the x-ray radiation. In the case of a plasma generated by a femtosecond laser pulse, the duration of the emitted x-ray burst can be comparable to that of the laser pulse, when certain conditions are met [8]. In this manner it is possible to generate femtosecond x-ray pulses.

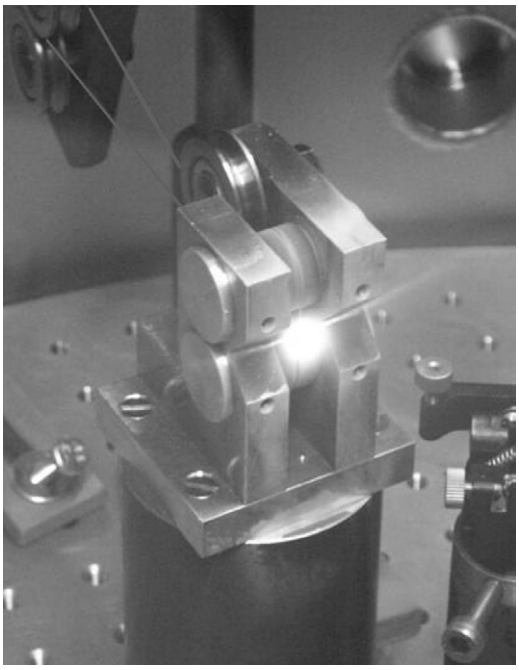

Figure 1. A photograph of the x-ray source. A laser beam coming from the left (not visible) is focused on a titanium wire producing the plasma plume visible in the centre of the picture. The incoming and outgoing wire can be recognized in the upper left corner.

Figure 1 shows a photograph of a laser plasma x-ray source. In this particular case laser pulses of 40 fs duration are focused onto a thin titanium wire which can be recognized in the upper left corner of figure 1. Because the laser is pulsed at a high repetition frequency, the wire must be rapidly pulled through the laser focus to avoid material erosion and the wire being cut. The peak laser intensity reaches 3×10^{16} W cm^{-2}. A spectrum of the x-ray emission from the titanium wire target is shown in figure 2. A large portion of the x-ray emission from the laser-produced plasma is titanium Kα radiation with a photon energy of 4.5 keV. The corresponding x-ray wavelength of 0.275 nm is just right for x-ray diffraction from crystal lattices. The x-ray wavelength can be easily changed simply by replacing the wire material. For example, with a copper wire one obtains Kα radiation from copper, $\lambda = 0.154$ nm (8 keV).

3. Focusing of the x-rays

The x-rays generated in this way are emitted incoherently into the full solid angle from a small spot on the target. The size of the emitting area is determined by the laser focal spot, which is typically 10 μm in diameter. To use this radiation for an experiment, one must try to collect as large a portion of the x-rays as possible and focus it onto the sample to be studied. X-rays can be effectively collected and focused using the x-ray Bragg reflection from the lattice plains of bent crystals [9]. To image the point-like x-ray source onto a sample we use toroidal mirrors in Rowland geometry as shown in figure 3. For one-to-one imaging of the source onto the sample the microplasma and the sample area (to be probed by the x-rays) should be located on the Rowland circle in a symmetrical configuration. Under these conditions the Bragg condition can be satisfied over almost the entire area of the x-ray mirror.

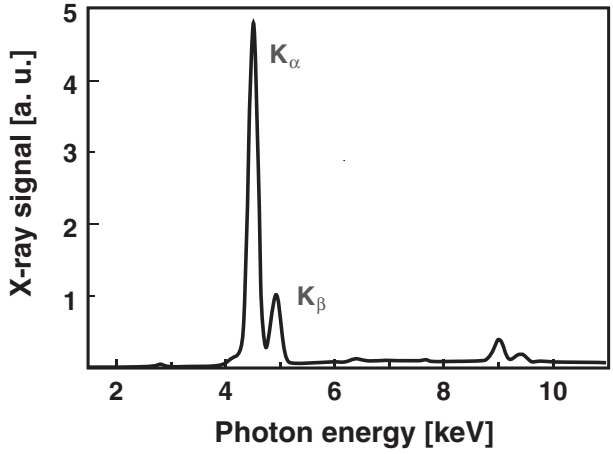

Figure 2. An x-ray emission spectrum of the titanium source driven at 1 kHz repetition rate with the Kα and the Kβ lines of titanium (Kα1 and Kα2 not resolved). The laser parameters are: 1.4 mJ, 40 fs, 3×10^{16} W cm^{-2}. The measured x-ray emission is 1.2×10^7 Kα photons per pulse into the full solid angle. The features near 9 keV are an artefact of the detector (multi-photon counts).

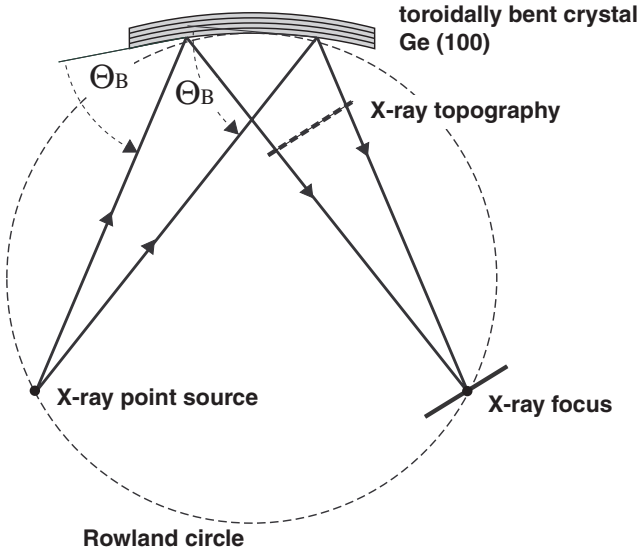

Figure 3. The Rowland circle geometry of the x-ray mirror using a toroidally bent Ge crystal platelet with (100) surface orientation and Bragg reflections from (400) lattice planes. The corresponding Bragg angle for titanium Kα radiation ($\lambda = 0.275$ nm) is 76.7°. The dashed line indicates (qualitatively) the position for the measuring spatial distribution of the reflected x-rays.

For titanium Kα radiation we use crystal platelets of Ge and GaAs with (100) orientation. Suitably oriented crystals are thinned down to less than 100 μm and then bonded to a toroidally shaped substrate surface. A photograph of a Ge(100) x-ray mirror for titanium Kα is depicted in figure 4. The Ge crystal has a rectangular shape with the approximate dimensions of 1.5 cm by 4 cm and radii of curvature of 50 and 45 cm in the horizontal and the vertical plane, respectively. Figure 5 shows spatial x-ray intensity distributions, measured by an

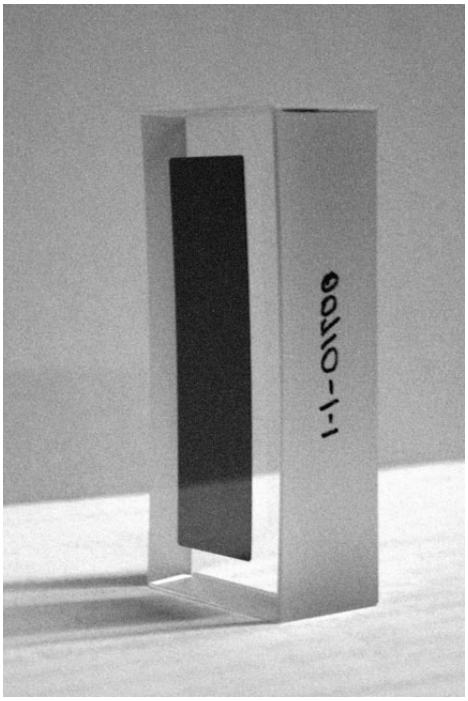

Figure 4. A photograph of an x-ray mirror with a Ge crystal bonded on the surface of a glass substrate. The x-ray mirror was manufactured by INRAD Inc., 181 LeGrand Avenue, Northvale, NJ 07647, USA.

x-ray-sensitive CCD camera. The spot diameter in the focal plane is less than 100 μm. Also shown in figure 5 is the out-of-focus spatial distribution closer to the mirror surface, where the intensity distribution outlines the shape of the reflecting Ge crystal. It can be seen that the x-ray distribution is quite homogeneous across the entire mirror surface with the exception of just a few localized imperfections.

When the x-ray plasma source is driven by femtosecond laser pulses of 100 mJ from a titanium–sapphire laser system ($\lambda = 800$ nm), there are approximately 5×10^4 Kα photons per pulse in the x-ray focal spot. Thus, with a repetition frequency of 10 Hz the x-ray flux is 10^6 Kα photons per second.

4. X-ray diffraction with femtosecond time resolution

With femtosecond x-ray pulses at our disposal x-ray experiments with femtosecond time resolution can be performed [10]. For example, to reveal ultrafast changes in the atomic structure ultrafast time-resolved x-ray diffraction experiments can be carried out using a variant of the well-known ultrafast optical spectroscopy pump–probe scheme in which the optical probe pulse is replaced by an x-ray pulse.

The optical pump/x-ray probe scheme is shown in figure 6. A femtosecond laser pulse from a titanium–sapphire laser system generates a microplasma on a suitable target. The x-rays from the plasma are collected by an x-ray mirror and focused on the sample to be studied. Suppose that we wish to study the structural changes triggered by an optical pump pulse. A suitable pulse can be produced by splitting a fraction off the main pulse and, if necessary,

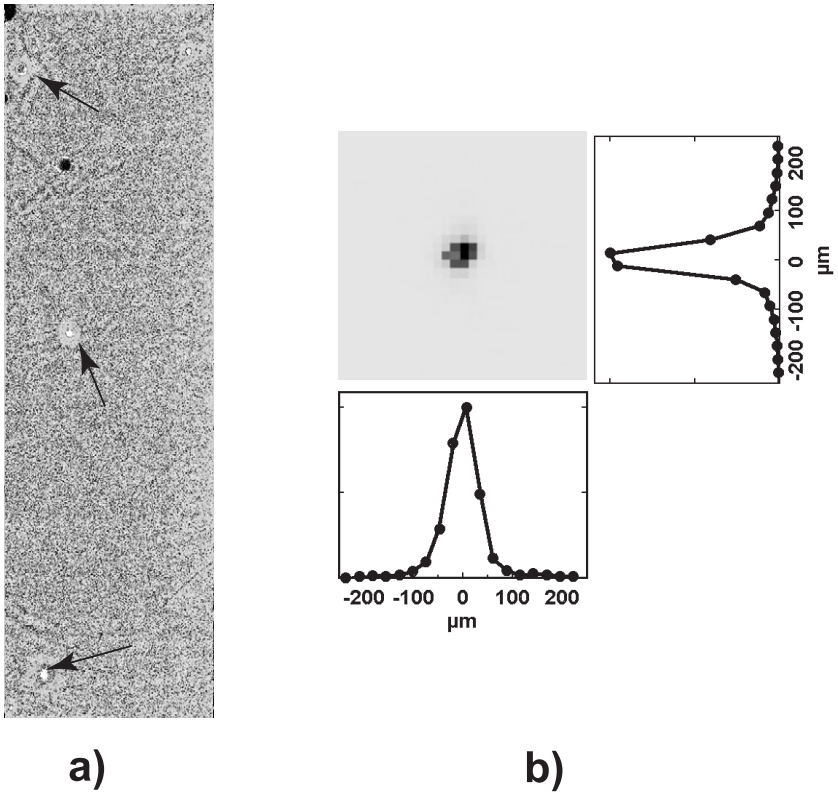

Figure 5. The spatial distribution of the reflected x-ray intensity. (a) The CCD camera close to the mirror (see figure 3). The arrows indicate local imperfections of the bonded crystal. (b) The camera in the focal plane. The size of the pixels that can be recognized in (b) is 20 μm by 20 μm. The measured widths (FWHM) of the horizontal and the vertical profiles are 60 and 70 μm, respectively.

changing its frequency, for instance by second-harmonic generation or some other non-linear optical frequency conversion scheme. By means of an optical delay line the time delay of the arrival of the probe pulse at the sample can be precisely controlled. The sample volume excited by the pump pulse must, of course, overlap the volume illuminated by the x-ray probe pulse.

The angular distribution of the diffracted x-rays can be measured with a suitable area detector, for example, an x-ray-sensitive CCD camera. By measuring the diffraction pattern as a function of the delay time between pump and probe, information on the evolution of the atomic structure may be recorded. There is no need for a fast x-ray detector because the time resolution is determined by the duration of the x-ray pulse and not by the response time of the detector.

5. Ultrafast structural phase transitions in semiconductors

There is strong evidence from optical data that in covalent semiconductors such as silicon, germanium and other similar ones, the photoexcitation of a high concentration of electrons and holes leads to a destabilization of the lattice and a transition to the liquid phase [11]. An example is shown in figure 7 where the density of electron–hole pairs obtained from

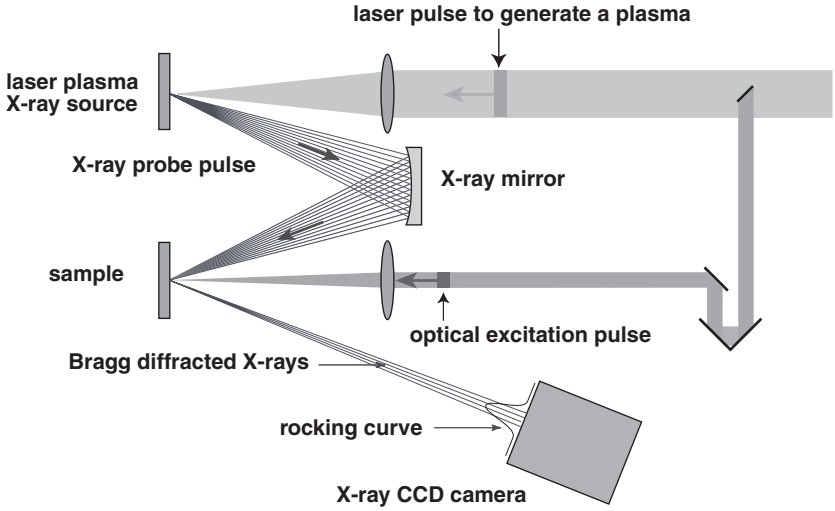

Figure 6. The optical pump/x-ray probe scheme for carrying out femtosecond time-resolved x-ray diffraction experiments.

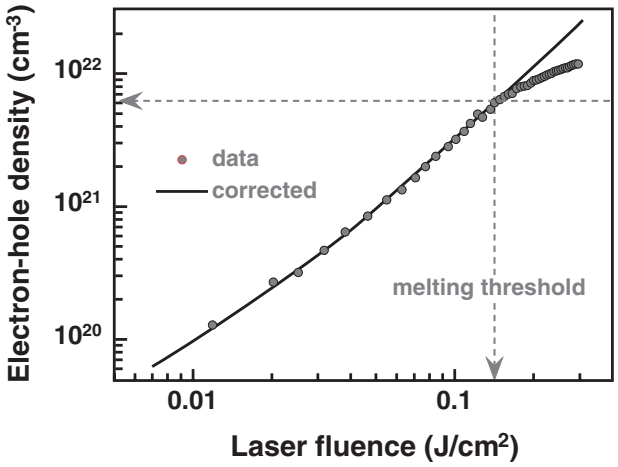

Figure 7. The electron–hole density generated by a 100 fs laser pulse at 620 nm in silicon. The density was obtained from measurements of the optical reflectivity. The corrected data take two-photon absorption into account.

measurements of the optical reflectivity of femtosecond laser-excited silicon is plotted as a function of the laser fluence. The data indicate that an electron–hole pair density of approximately 10^{22} cm^{-3} is reached at approximately 150 mJ cm^{-2}. At this high level of excitation, an abrupt increase in the optical reflectivity is observed to occur within a few hundred femtoseconds after the excitation pulse. As an example of the induced changes in the optical reflectivity, a series of reflectivity spectra of silicon measured at various delay times after laser excitation are depicted in figure 8. The dashed–dotted and the dashed lines represent the well-known reflectivity spectra of crystalline and molten silicon, respectively. The measured time-dependent reflectivity data show that within a few hundred femtoseconds the reflectivity spectrum changes from crystalline type to liquid type.

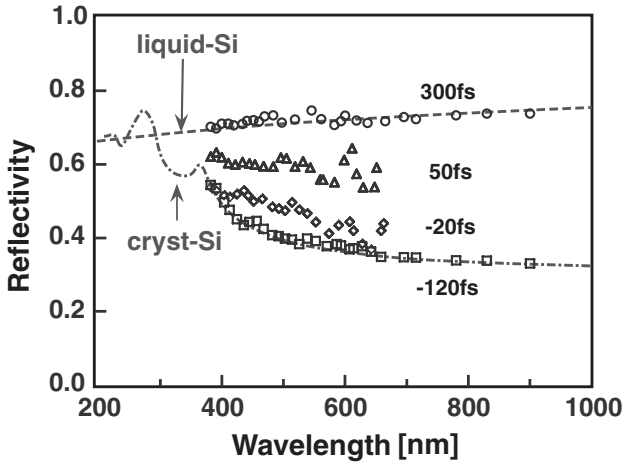

Figure 8. Spectra of the optical reflectivity of silicon. Dash–dotted curve: crystalline silicon. Dashed line: molten silicon. Data points: spectra measured at various time delays between the pump pulse and the optical probe pulse (optical pump/optical probe measurements).

The changes in the reflectivity spectra suggest that a transition from the covalent crystalline state to the metallic liquid state is taking place. Such ultrafast structural phase transitions [12] have been extensively investigated in the past by means of ultrafast optical spectroscopy. It is fundamentally different from ordinary thermal melting which takes much longer. Because the electronically induced solid-to-liquid transition is accomplished in a time much shorter than that required for the thermalization of the deposited laser energy, this melting process is also called *non-thermal melting*.

6. Probing of structural phase transitions by x-ray diffraction

Femtosecond laser-induced non-thermal melting obviously represents an excellent case study for the application of ultrafast x-ray diffraction and the demonstration of its feasibility [13]. However, there is a principal experimental difficulty because x-rays tend to penetrate deeply into the bulk of a material, whereas the laser melting of semiconductors produces a very thin liquid layer on the surface, typically less than 100 nm. When the lattice is destroyed by the melting process the x-ray diffraction from the lattice planes must evidently disappear completely. If, however, the penetration depth of the x-rays is much greater than the thickness of the liquid layer on the surface, the x-ray diffraction will be dominated by the solid bulk material underneath the liquid. Under these circumstances, no significant change in the x-ray diffraction signal would be expected upon melting.

Figure 9 illustrates how the problem due to the mismatch of the penetration depths can be avoided by using special heteroepitaxial semiconductor samples. It is possible to grow thin crystalline layers of germanium on silicon substrates of (111) orientation using a surfactant-mediated growth process which relieves the stress at the interface [14]. The important point is that a high quality heterostructure is obtained in which the lattice constants of the germanium layer and of the silicon substrate do not match. Thus, the Bragg angles for x-ray diffraction from the Ge layer and the Si substrate are different, and x-ray diffraction from the Ge layer and the substrate can be readily distinguished.

The Ge–Si heterostructures are very suitable for studies of the changes in the atomic structure associated with femtosecond laser-induced melting using time-resolved x-ray

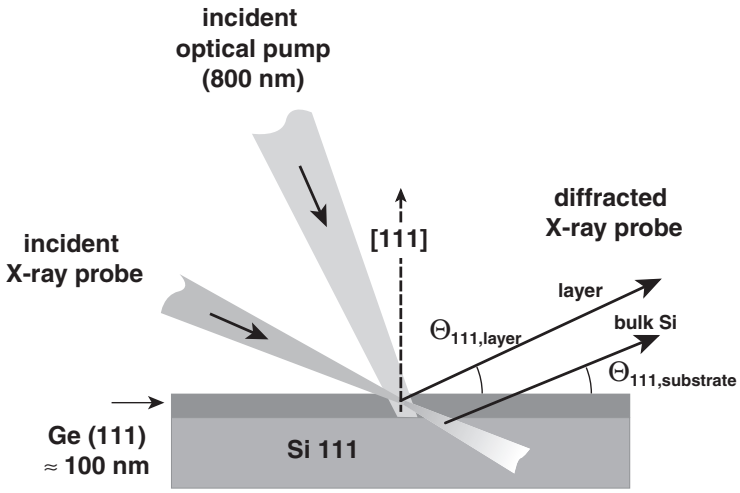

Figure 9. Heteroepitaxial Ge-on-Si samples for optical pump/x-ray probe measurements indicating the selective optical pumping and x-ray probing of the Ge layer.

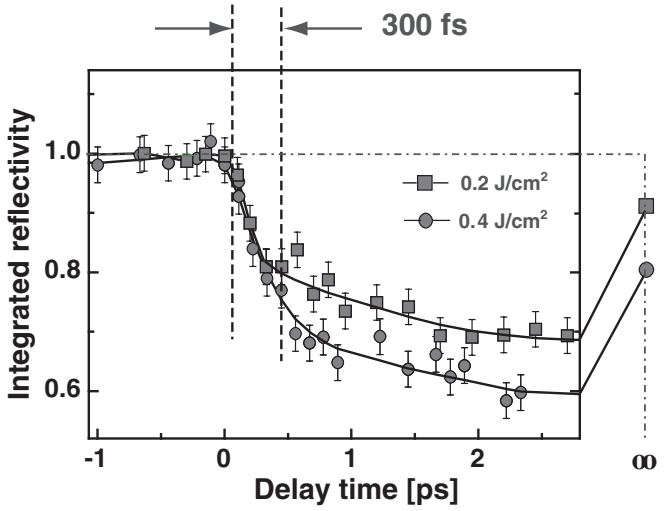

Figure 10. X-ray diffraction from the (111) lattice planes of Ge versus time delay for two different energy fluences of the pump pulse ($\lambda = 800$ nm).

diffraction [15]. Germanium has a secondary direct bandgap of approximately 0.8 eV and therefore absorbs quite strongly at the wavelength of the titanium–sapphire laser (800 nm) while silicon absorbs only weakly at this wavelength. Thus, it is possible to selectively deposit laser energy in the germanium layer causing it to melt, and also to selectively probe the Ge lattice with the x-rays.

Figure 10 shows the results of time-resolved x-ray diffraction experiments [15]. The x-ray diffraction signal (integrated reflectivity) measured from the (111) lattice planes of Ge is plotted as a function of the delay time between the x-ray probe pulses and the laser pump pulses for two different laser fluences. Negative times indicate the arrival of the laser pump pulse after the x-ray probe pulse. In this case, the lattice is still intact when the x-ray pulses interact with the

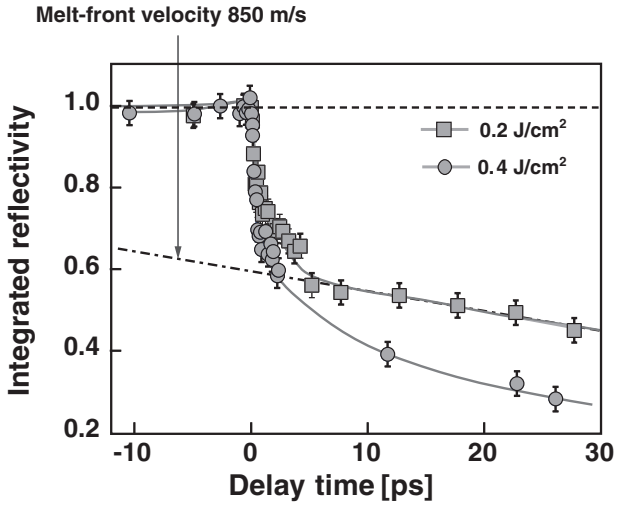

Figure 11. X-ray diffraction from the (111) lattice planes of Ge versus time delay for two different energy fluences of the pump pulse ($\lambda = 800$ nm). Evolution on the picosecond timescale. Melt front velocity: see the text.

sample and the diffraction remains unchanged. However, a distinct decrease in the diffraction is observed after the arrival of the pump pulse. This initial decrease takes approximately 300 fs but thereafter the decrease of the x-ray diffraction signal continues at a much slower rate. However, although the diffraction signal becomes weaker, it never disappears completely. A portion of the 170 nm thick germanium layer remains crystalline because in this case the laser energy employed is not enough to melt the entire layer.

Measurements of the x-ray diffraction at very long delay times (delay time 'infinity' in figure 10), after complete resolidification of the molten layer, indicate that the diffraction signal recovers almost completely. More detailed investigations show that an epitaxial regrowth takes place and that the Ge crystalline layer is restored. However, it has been found that a certain amount of material is removed by laser ablation, typically 10–20 nm, depending on the laser fluence. The recrystallized Ge layer is thinner than the original one and the recovery of the x-ray diffraction signal is therefore incomplete.

Two main conclusions can be drawn from the results of the x-ray diffraction measurements during the first picosecond:

(i) The fast initial decrease in the diffraction signal is consistent with the interpretation of the optical reflectivity results that a portion of the Ge crystal undergoes disordering within a few hundred femtoseconds. The measured 25% decrease in the diffraction indicates the development of a molten layer of approximately 40 nm thickness.
(ii) The observed fast decay of the diffraction signal puts an upper limit on the duration of the x-ray pulses of about 300 fs.

Previously, the only alternatives for measuring the duration of the x-ray pulses from laser-produced plasmas were streak cameras, but in this case the time resolution is only about one picosecond.

Interesting insight into laser-induced melting processes can be obtained from more detailed measurements of the x-ray diffraction over a large range of delay times. Figure 11 shows the evolution of the x-ray diffraction signal over an extended range up to 30 ps. It can be seen that

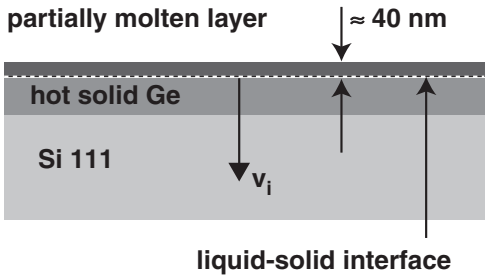

Figure 12. A schematic diagram illustrating the various strata of the excited sample: liquid layer, hot crystalline Ge, silicon substrate. V_i is the propagation velocity of the liquid–solid phase boundary (melt front velocity).

the first fast decay of the diffraction efficiency is followed by an approximately linear decrease over tens of picoseconds.

For an interpretation of this observation consider figure 12. The initial ultrafast, non-thermal melting leaves a very hot liquid layer of approximately 40 nm on top of solid material. Heat is transferred from the hot liquid to the underlying solid material causing more material to melt and leading to an increase in the thickness of the molten layer. The x-ray measurements indicate that the liquid–solid interface propagates towards the inside with a velocity of about $v_i = 850$ m s^{-1}. This large melt front velocity suggests that a rapid thermal melting process under highly superheated conditions is taking place.

7. X-ray rocking curves and picosecond acoustic transients

The x-ray signal plotted in figures 10 and 11 is the 'integrated reflectivity' of a particular Bragg reflection (h, k, l), that is, the diffracted x-ray radiation integrated over the angular distribution. The angular profiles are called 'rocking curves'. In this section we show that the rocking curves provide important additional information [15]. In particular, interesting insight into the acoustic processes that follow the structural phase transition on a picosecond timescale can be obtained.

Figure 13 illustrates the measurement of rocking curves. The cone of x-rays that is incident on the sample from the x-ray mirror typically covers an angular range of a few degrees, depending on the width of the mirror and its distance from the x-ray source. On the other hand, the angular width $\Delta\Theta$ of the usual rocking curves is much smaller. Thus, the full rocking curve can be recorded with a suitable area detector such as a CCD camera, and it is possible to monitor, for example, changes in the position and the width of the rocking curves.

Figure 14 depicts examples of rocking curves of the (111) Bragg orders of Ge and Si measured at four different time delays. The dashed lines represent the rocking curves of the Ge layer and the Si substrate for the unperturbed materials. The solid lines represent the rocking curves after laser excitation. The data for a short time delay of 0.8 ps show that the shape and the position of the rocking curve remain unchanged; there is only a reduction in the diffraction intensity of Ge to somewhat less than 70%. This subpicosecond change in the x-ray diffraction is attributed to the ultrafast structural phase transition as discussed in the previous section.

On the other hand, complex changes both in the strength and the angular profile are observed for picosecond time delays. These observations can be qualitatively explained as follows. After ultrafast melting and thermalization of the deposited optical energy the surface

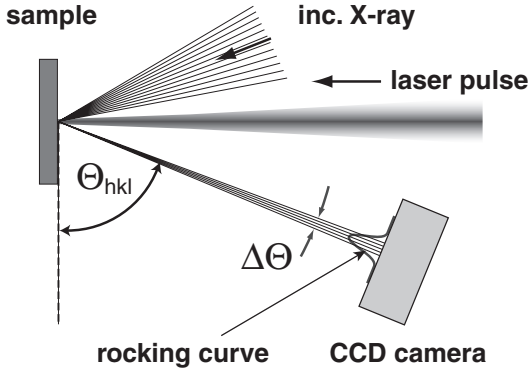

Figure 13. A schematic diagram illustrating the measurement of the angular distribution (rocking curve) of the Bragg-reflected x-ray probe pulse. Θ_{hkl} is the Bragg angle for the diffraction from the lattice planes (h, k, l). $\Delta\Theta$ indicates the angular width of the rocking curve.

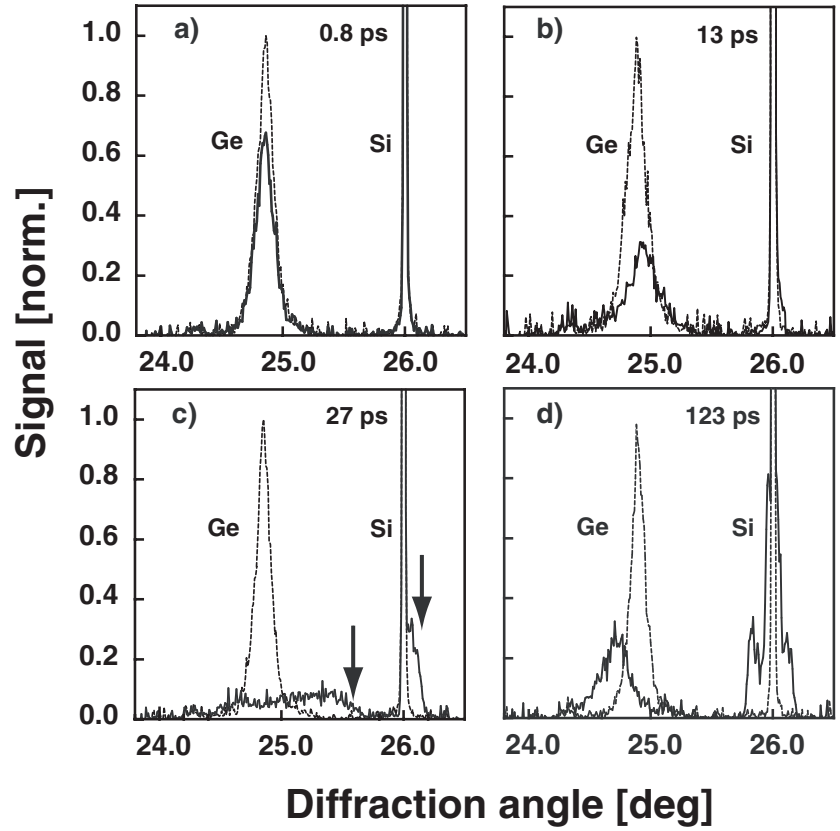

Figure 14. Full line: measured rocking curves for various time delays. Dashed lines: rocking curves of the unperturbed sample (no laser excitation).

of the sample is covered by a layer of hot, pressurized molten Ge (figure 12). Underneath the liquid there is an intact layer of crystalline Ge, also hot and at high pressure. By comparison, the pressure in the underlying Si substrate is negligible because at 800 nm the optical absorption in Si and thus the deposited energy is much less than in Ge.

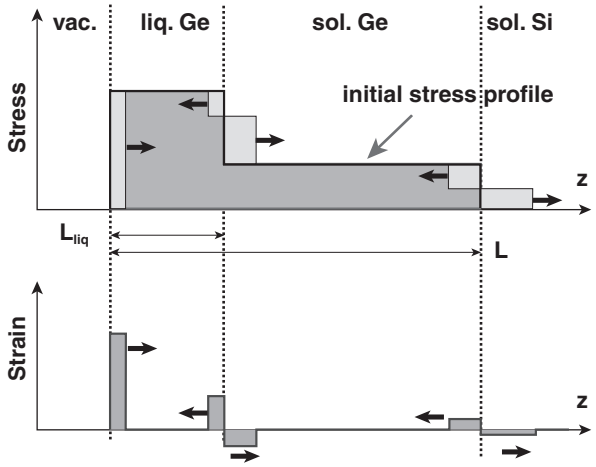

Figure 15. A schematic diagram illustrating the qualitative stress and strain profiles.

The initial stress/pressure imbalance at the interfaces triggers several acoustic perturbations. It follows from the continuity-of-stress condition that a compressive and an expansive strain wave is launched from each interface into the low pressure and the high pressure side, respectively. Also, a rarefaction wave develops at the surface and travels into the liquid. Figure 15 shows a qualitative picture of the developing stress and strain waves. The initial pressure is expected to be at its highest in the molten surface layer because the largest portion of the optical energy is deposited approximately 40–50 nm beneath the surface. Therefore, the primary acoustic perturbation in the remaining crystalline Ge should be compressive strain launched from the molten layer.

In addition to the acoustic perturbations, the liquid-to-solid interface (melt front) moves forward into solid Ge as discussed in the foregoing section. The liquid layer grows at the expense of the crystalline layer, resulting in a continuing overall reduction in the diffraction efficiency.

The different acoustic perturbations do not overlap for periods shorter than the travel time between the interfaces (e.g. 23 ps for 130 nm of solid Ge). Later on, however, reflections occur at the various interfaces because of the mismatch of the acoustic impedance. The situation becomes quite complicated until the acoustic transients have finally damped out.

According to this qualitative model, the first acoustic effects to be noticed should be a compression in Ge and, to a lesser extent, also in Si. The rocking curve for 13 ps (figure 14(b)) shows that this is indeed observed. There is a clear shift of the Ge line towards larger diffraction angles and a weak shoulder of the Si curve in the same direction.

The rarefaction wave approaching from the liquid surface is expected to affect the crystalline layer after times $t > L_{\mathrm{liq}}/c_{\mathrm{liq}} \approx 15$ ps, where $c_{\mathrm{liq}} = 2660\ \mathrm{m\ s^{-1}}$ is the sound velocity of liquid Ge. In fact, the Ge rocking curve at 27 ps (figure 14(c)) develops a new side band at lower diffraction angles and exhibits a doubly peaked structure. This shape indicates the presence of both compressed and expanded strata in Ge at this time.

The data in figure 14 can be used to obtain an estimate of the stress/pressure associated with the acoustic perturbations. For example, consider the positive angular shifts $\Delta\Theta$ marked by the arrows in figure 14(c). They indicate compressive strain $\varepsilon = \Delta\Theta/\tan\Theta_{\mathrm{B}}$ of -0.02 and -0.005 in Ge and Si, respectively. The transient stresses $\sigma = \rho \mathsf{c}_{111}^2 \varepsilon$ (ρ: density; c_{111}: speed of sound in the (111) direction) obtained from these numbers are 3.3 and 1 GPa.

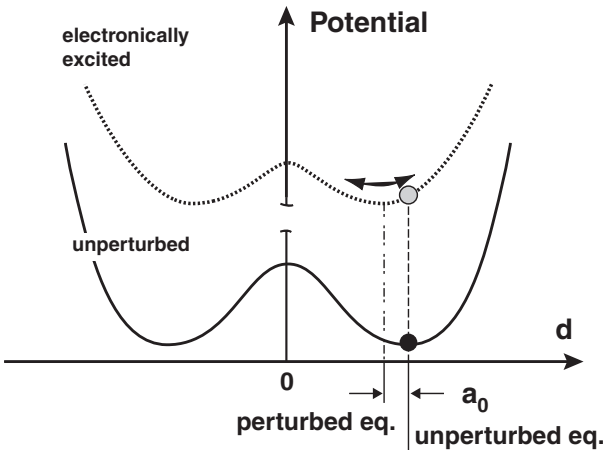

Figure 16. A schematic diagram illustrating displacive excitation in bismuth. A qualitative plot of the potential energy as a function of d, the displacement of the second Bi atom from the centre of the unit cell. Full curve: the unperturbed system. The black dot marks the equilibrium position. Dotted curve: the potential energy of the electronically excited system. The grey dot marks the new equilibrium point. In the electronically excited state the atom (grey dot) relaxes by performing oscillations around the perturbed equilibrium position. The change in d is denoted a_0 which is the initial oscillation amplitude.

Finally, the data for 123 ps (figure 14(d)) reveal further points of interest. At this late stage the acoustic perturbations of the Ge layer have damped out leaving the relaxed, thermally expanded material, as indicated by a shift of the diffraction profile to smaller angles. The shift represents a thermal expansion of $\varepsilon_{\mathrm{th}} = 0.008$, which would correspond to a temperature of approximately 1100–1200 K. This value is close to the melting temperature of Ge, suggesting that the liquid and the solid Ge have reached equilibrium near the melting point. As regards the rocking curve of Si at 123 ps, both expansive and compressive strain can be clearly recognized. This complex structure is presumably attributable to transient bipolar strain superimposed on the thermal expansion profile of Si.

8. Coherent lattice vibrations

The transitions from the crystalline solid state to the disordered liquid state involve a complete rearrangement of the atomic structure causing the x-ray diffraction from the lattice planes to vanish completely. However, even using today's laser plasma x-ray sources with relatively low x-ray flux, more subtle changes in the atomic configuration such as the changes associated with vibrations of the atoms in a crystal lattice may also be observed, as has been shown in experiments using the semimetal bismuth [16].

The usual crystal structure of Bi is a slightly distorted face-centred cubic lattice with two atoms in the primitive unit cell. If the lattice is chosen in such a way that the first Bi atom is positioned on a lattice point, then the second Bi atom is located on the body diagonal slightly displaced from the centre of the unit cell.

The crystal symmetry permits totally symmetric lattice vibrations [17]. We are particularly interested in the totally symmetric *optical* mode which corresponds to an internal vibration of the atoms in the unit cell with the two Bi atoms moving against each other along the body diagonal (A_{1g} optical phonon mode). It is well known that this mode can be excited by the so-called displacive excitation mechanism [17] which is illustrated in figure 16. This qualitative plot shows the potential energy of the unperturbed (full curve) and of the electronically excited

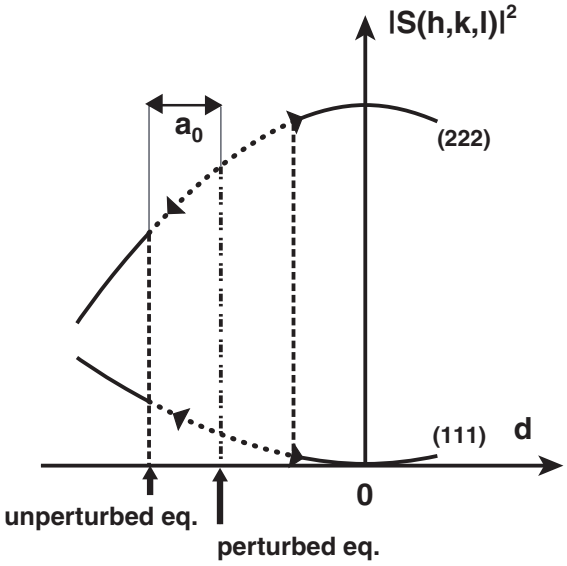

Figure 17. The squared modulus of the geometrical structure factor $|S(h, k, l)|^2$ of Bi as a function of the displacement d (for the definition see the caption of figure 16) for (111) and (222) Bragg reflections. A movement towards the centre of the unit cell leads to an increase in the (222) and a decrease in the (111) case. Atomic oscillations lead to cyclical changes in the x-ray diffraction.

crystal (dotted curve) as a function of distance d of the second Bi atom from the centre of the unit cell. In the unperturbed crystal d has a certain equilibrium value slightly different from half the length of the body diagonal. The important point is that the equilibrium atomic distance can be easily changed by many kinds of perturbation, for example, electronic excitation.

Suppose that the crystal is electronically excited by a short laser pulse. The potential energy curve is now qualitatively given by the dotted curve in figure 16. The equilibrium distance assumes a new value. Immediately after the excitation the atoms find themselves in a displaced position with respect to the perturbed equilibrium. The atoms relax by performing a damped oscillation around the new equilibrium. This atomic motion occurs *in phase* in all unit cells, and thus a coherent optical phonon mode with a wavevector $q = 0$ is established.

How can the resulting collective atomic motion be detected by means of time-resolved x-ray diffraction? Consider the geometrical structure factor $S(h, k, l)$ of Bi for the (111) and the (222) Bragg reflections as a function of the distance of the Bi atoms shown in figure 17. The square modulus $|S(h, k, l)|^2$ is proportional to the diffraction signal for the Bragg reflection corresponding to a set of Miller indices (h, k, l). As pointed out above, in the unperturbed crystal the second Bi atom is slightly displaced from the centre. The excitation is expected to change the location of the equilibrium point. Figure 17 shows that an increase in the (222) x-ray diffraction is expected if the atoms move towards a new equilibrium located closer to the centre. However, for the (111) diffraction the same motion should lead to a decrease. Thus, the oscillations of the atoms associated with the displacively excited coherent optical phonon mode should give rise to periodic changes in the x-ray (222) diffraction and similar oscillations in the (111) diffraction, but 180° out of phase.

Fortunately, crystalline Bi films can also be grown as heterostructures on (111) Si substrates, which allows the actual experimental observation of displacively excited coherent optical phonons in Bi. Because of the different lattice constants, the Bragg angles for the

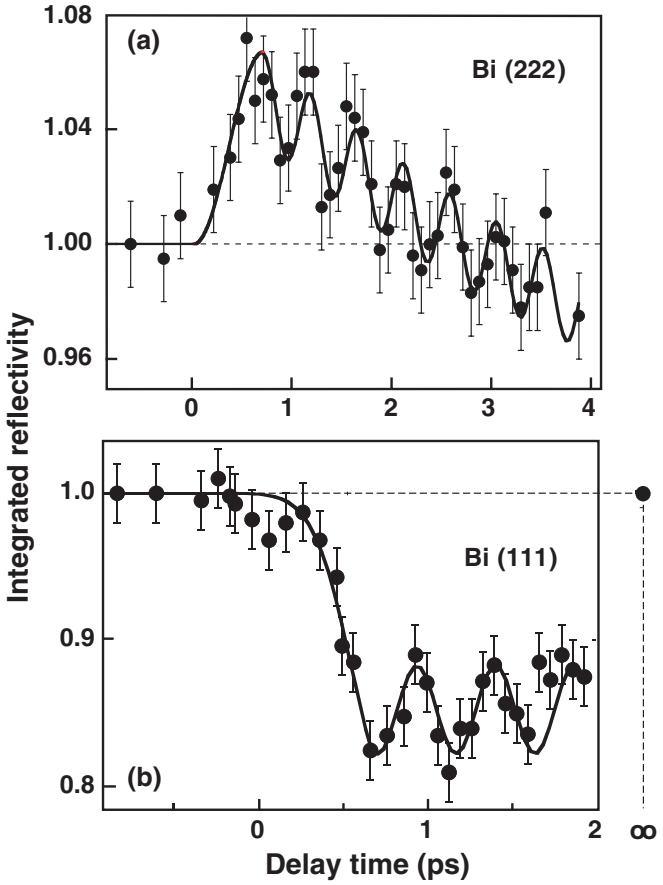

Figure 18. The measured x-ray diffraction signal from (a) (222) and (b) (111) lattice planes of Bi as a function of the time delay. The solid curves are guides to the eye.

diffraction from the Bi film and the Si substrate are different, and it is possible to selectively probe the Bi films with the x-ray pulses.

Results of time-resolved x-ray diffraction measurements on a femtosecond laser-excited Bi film of 50 nm thickness are depicted in figure 18. After the arrival of the laser excitation pulse the x-ray diffraction signal from (222) lattice planes (figure 18(a)) shows an initial increase, suggesting that the off-centre Bi atoms do indeed move closer to the centre of the unit cell, i.e. the Bi–Bi distances increase. This initial increase in the x-ray diffraction signal is followed by distinct oscillations. Thus, the observed evolution of the diffraction is consistent with the expected atomic response to the perturbation of the equilibrium position.

If the microscopic interpretation in terms of a collective atomic motion is correct, the signal for (111) diffraction should exhibit an initial decrease followed by oscillations out of phase with those observed in the (222) diffraction. The results of figure 18(b) indicate that this is indeed the case. Thus, the picture emerging from the time-resolved x-ray diffraction data for two different Bragg orders is consistent and provides clear evidence of the excitation of coherent lattice vibration on an atomic scale.

Interesting conclusions concerning the frequency and the atomic displacements can be drawn. The measured period (frequency) of the oscillations both in the (222) and the (111) diffraction signals is 470 fs (2.14 THz) which is interpreted as the oscillation period

of the excited optical phonon mode. The oscillation period (vibrational frequency) of the totally symmetric A_{1g} optical phonon mode of unperturbed Bi is 347 fs (2.92 THz). This comparison indicates that an important decrease of the vibrational frequency is observed for strong femtosecond laser excitation (6 mJ cm^{-2}).

It is interesting to estimate the actual atomic displacements under these conditions. According to figure 17, the observed variations in the x-ray diffraction signal are related to the changes in the Bi–Bi distance. The values of the atomic displacements estimated from the experimental data are approximately 0.015–0.02 nm. These values represent a significant fraction of the nearest neighbour distance which is 0.35 nm, indicating that coherent vibrations with very strong excursions of the atoms are generated. The observed decrease in the oscillation frequency is probably due to both anharmonicity and modification of the atomic potentials caused by the electronic excitation [18]. Experiments with a high level of laser excitation produced still larger shifts of the oscillation frequency down to approximately 1 THz. After this the atomic motion transforms into an aperiodic mode and a phase transition to the liquid state of Bi occurs.

9. Incoherent lattice vibrations

The interaction between electrons and lattice vibrations plays an important role in solid state physics. For example, optical absorption excites the electrons from the electronic ground state to higher energy states of the material. The excited electrons relax very rapidly by transferring their excess energy to lattice vibrations. The final result of the electronic relaxation is an increase in the temperature of the material.

Electronic relaxation processes have been studied quite extensively using ultrafast time-resolved optical spectroscopy [19]. For example, it is possible to observe the initial thermalization among the electrons and the subsequent cooling of the electronic system caused by the energy transfer to the lattice. However, to a large extent the observation of the build-up of lattice vibrations associated with the electronic energy relaxation has been elusive, and there are only a few examples of the detection of the lattice vibrations generated in an electronic relaxation process [20]. Now time-resolved x-ray diffraction is offering new opportunities for detecting the excitation of lattice vibrations caused by relaxing electrons.

In the electronic relaxation process the energy is redistributed incoherently over a large number of vibrational lattice modes. As a result, the individual atoms perform random oscillations around their equilibrium lattice position. It is well known that such incoherent lattice vibrations affect the Bragg diffraction of x-rays from the lattice planes in the following manner. While the position and the profile of the Bragg peaks do not change, their intensity diminishes by a certain factor, the so-called Debye–Waller factor [21]. The Debye–Waller factor is an exponential function of the mean square atomic displacement which is proportional to the lattice temperature under thermal equilibrium conditions.

Using a suitably short x-ray pulse the instantaneous value of the Debye–Waller factor can be measured by means of x-ray diffraction. Thus, it is possible to observe the evolution of the Debye–Waller factor and watch the lattice temperature rise during the electronic relaxation that follows an optical excitation of the material.

For a first demonstration of the feasibility of such experiments we have used the Ge/Si heterostructures discussed previously. Apart from choosing a level of laser excitation well below the melting threshold, the experimental procedure is very similar to the one used in the melting experiments. Femtosecond laser pulses of 800 nm wavelength were employed for photoexciting electron–hole pairs in the Ge layer, and the x-ray diffraction from (400) lattice planes of the excited sample (integrated reflectivity) was measured as a function of

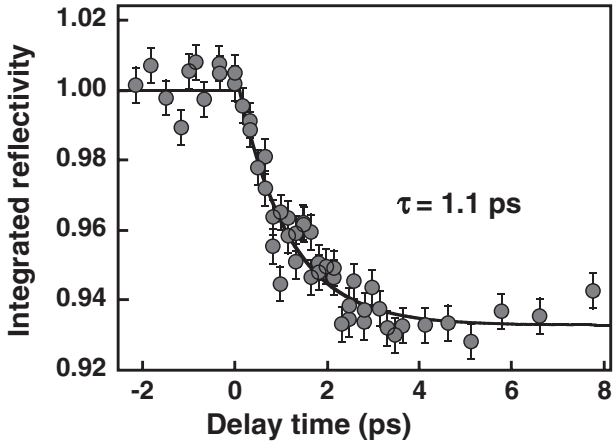

Figure 19. X-ray diffraction from the (400) lattice planes of Ge plotted versus time for weak laser excitation (below the melting threshold). A (111) Ge–Si heteroepitaxial sample.

the delay time between the x-ray probe pulses and the laser pulses. The result is depicted in figure 19. High measuring accuracy is required because under the given experimental conditions the Debye–Waller effect is fairly weak. For a laser energy fluence of 35 mJ cm^{-2}, a decrease in the x-ray diffraction signal down to 93% of the signal without laser excitation is observed. The measured decrease of the x-ray diffraction signal represents an increase in the lattice temperature from room temperature to 550 K. Considering the heat capacity of Ge, the temperature rise deduced from the x-ray data agrees very well with the final temperature estimated from the amount of absorbed laser energy.

The electron–phonon energy relaxation time of Ge is obtained from the measured time dependence of the Debye–Waller effect. The experimental data can be represented by an exponential function with a time constant $\tau = 1.1$ ps. Thus, we conclude that in germanium the optically deposited energy is transferred to lattice vibrations in just about one picosecond. This result is in good agreement with the expected general time range for energy exchange between electrons and phonons.

10. Summary and conclusions

In this article we have shown that laser plasmas produced by intense femtosecond pulses emit subpicosecond bursts of kilovolt x-rays. It has been demonstrated that these x-ray pulses can be used for optical pump/x-ray probe experiments, enabling the extension of ultrafast spectroscopy to the x-ray regime. In particular, we have used time-resolved x-ray diffraction to study laser-induced structural phase transitions in semiconductors and confirmed previous conclusions from optical experiments that solid-to-liquid transitions can occur in only a few hundred femtoseconds. We were able to observe the dynamics of picosecond acoustic perturbations generated during the relaxation of the hot pressurized liquid layer produced by ultrafast melting. It was shown that much weaker changes in the atomic configurations can also be measured. The collective atomic motion associated with a displacively excited coherent optical phonon mode was detected and the atomic oscillation cycle of the lattice vibration could be resolved. Finally, time-resolved measurements of the Debye–Waller effect revealed the heating of the crystal lattice resulting from the energy relaxation of photoexcited electrons and holes, and the electron–phonon energy transfer time was measured.

Although quite a large number of interesting new kinds of investigations can be performed using laser plasma x-ray sources the limitations of such sources are rather obvious. For instance, there are restrictions on the available x-ray flux, and it is difficult to produce a highly collimated x-ray beam. On the other hand, large scale efforts to build new kinds of powerful electron accelerator based femtosecond x-ray sources are under way worldwide, for example the Linac Coherent Light Source (LCLS) project [22] at Stanford, USA, and the European x-ray laser project XFEL [23] at DESY, Hamburg, Germany. In addition to the exciting applications of x-ray free electron lasers, these developments will undoubtedly also greatly enhance the possibilities of femtosecond x-ray spectroscopy. On the other hand, great progress has also been made in the generation and application of ultrashort electron pulses [24], and subpicosecond electron diffraction has recently been used to study the dynamics of femtosecond laser-induced melting of aluminium films [25].

The femtosecond time regime is scientifically very important because it is the fundamental timescale of changes in atomic configurations. Over the last two decades femtosecond optical spectroscopy has made a great impact on many fields of science and technology. Femtosecond x-ray and electron pulses now enable a combination of ultrafast spectroscopy and structural science. Considering the fundamental scientific importance of the structure sciences, it is quite possible that this marriage could stimulate major new scientific developments.

Acknowledgments

This work was supported by the Deutsche Forschungsgemeinschaft in the programmes SPP 1153 and SFB 616. We also acknowledge support from the European Union in the framework of the XPOSE network. We are greatly indebted to Ch Blome, J Blums, A Cavalleri, M Horn-von Hoegen, M Kammler, M Nicouls, U Shymanovitch and A Tarasevitch, for their contributions to this work. The authors wish to thank E Förster and I Uschmann at the University of Jena for supplying one of the x-ray mirrors used in this work.

References

[1] Friedrich W, Knipping P and von Laue M 1912 *Sitz.ber., Kgl. Bayer. Akad. Wiss.* 303–22
Friedrich W, Knipping P and von Laue M 1913 *Ann. Phys., Lpz.* **41** 971
von Laue M 1912 *Sitz.ber., der Kgl. Bayer. Akad. Wiss.* 363–73
von Laue M 1913 *Ann. Phys., Lpz.* **41** 989
[2] Watson J D and Crick F H C 1953 *Nature* **171** 737–8
[3] Service R F 2002 *Science* **289** 1356
[4] Backhaus S, Dufee Ch G, Murnane M and Kapteyn H C 1998 *Rev. Sci. Instrum.* **69** 1207
Pittman M, Ferré S, Rousseau J P, Notebaert L, Chambaret J P and Chériaux G 2002 *Appl. Phys.* B **74** 529
[5] Kruer W L 2003 *Phys. Plasmas* **10** 2087
[6] Mourou G A, Barty C P J and Perry M D 1998 *Phys. Today* (January) 22–8
Umstadter D 2001 *Phys. Plasmas* **8** 1774
[7] Kühlke D, Herpers U and von der Linde D 1987 *Appl. Phys. Lett.* **15** 1785
Kmetec J D, Gordon C L III, Macklin J J, Lemoff B E, Brown G S and Harris S E 1992 *Phys. Rev. Lett.* **68** 1527
Rousse A, Audebert P, Geindre J P, Falliès F, Gauthier J C, Mysyrowicz A, Grillon G and Antonetti A 1994 *Phys. Rev.* E **50** 2200
Kieffer J C, Jiang Z, Ikhlef A and Cote C Y 1996 *J. Opt. Soc. Am.* B **13** 132
Guo T, Spielmann Ch, Walker B C and Barty C P J 2001 *Rev. Sci. Instrum.* **72** 41
[8] Reich Ch, Gibbon P, Uschmann I and Förster E 2000 *Phys. Rev. Lett.* **84** 4846
[9] Missalla T, Uschmann I, Förster E, Jenke G and von der Linde D 1999 *Rev. Sci. Instrum.* **70** 1288–99
[10] Rischel C, Rousse A, Uschmann I, Albouy P-A, Geindre J P, Audebert P, Gauthier J-C, Förster E, Martin J-L and Antonetti A 1997 *Nature* **390** 490
[11] Shank C V, Yen R and Hirlimann C 1983 *Phys. Rev. Lett.* **50** 454

Shank C V, Yen R and Hirlimann C 1983 *Phys. Rev. Lett.* **51** 900
Saeta P, Wang J-K, Siegal Y, Bloembergen N and Mazur E 1991 *Phys. Rev. Lett.* **67** 1023
Huang L, Callan J P, Glezer E N and Mazur E 1998 *Phys. Rev. Lett.* **80** 185
Sokolowski-Tinten K, Bialkowski J and von der Linde D 1995 *Phys. Rev.* B **51** 14186
Sokolowski-Tinten K, Bialkowski J, Boing M, Cavalleri A and von der Linde D 1998 *Phys. Rev.* B **58** R11805
[12] Stampfli P and Bennemann K H 1990 *Phys. Rev.* B **42** 7163
Stampfli P and Bennemann K H 1992 *Phys. Rev.* B **46** 10686
Stampfli P and Bennemann K H 1994 *Phys. Rev.* B **49** 7299
[13] Chin A H, Schoenlein R W, Glover T E, Balling P, Leemans W P and Shank C V 1999 *Phys. Rev. Lett.* **83** 336
Siders C W, Cavalleri A, Sokolowski-Tinten K, Toth C, Guo T, Kammler M, Horn-von Hoegen M, Wilson K R, von der Linde D and Barty C P J 1999 *Science* **286** 1340
Lindenberg A M, Kang I, Johnson S L, Missalla T, Heimann P A, Chang Z, Larsson J, Bucksbaum P H, Kapteyn H C, Padmore H A, Lee R W, Wark J S and Falcone R W 2000 *Phys. Rev. Lett.* **84** 111
Rousse A, Rischel C, Fourmaux S, Uschmann I, Sebban S, Grillon G, Balcou P, Förster E, Geindre J P, Audebert P, Gauthier J C and Hulin D 2001 *Nature* **410** 65
Feurer T, Morak A, Uschmann I, Ziener C, Schwoerer H, Reich C, Gibbon P, Förster E, Sauerbrey R, Ortner K and Becker C R 2002 *Phys. Rev.* E **65** 16412
[14] Horn-von Hoegen M, Le Goues F K, Copel M, Reuter M C and Tromp R M 1991 *Phys. Rev. Lett.* **67** 1130
[15] Sokolowski-Tinten K, Blome Ch, Dietrich C, Tarasevitch A, von der Linde D, Horn-von Hoegen M, Cavalleri A, Squier J A and Kammler M 2001 *Phys. Rev. Lett.* **87** 225701
[16] Sokolowski-Tinten K, Blome C, Blums J, Cavalleri A, Dietrich C, Tarasevitch A, Uschmann I, Förster E, Horn-von Hoegen M and von der Linde D 2003 *Nature* **422** 287–9
[17] Zeiger H J, Vidal J, Cheng T K, Ippen E P, Dresselhaus G and Dresselhaus M S 1992 *Phys. Rev.* B **45** 768–78
[18] Hase M, Kitajima M, Nakashima S and Mizoguchi K 2002 *Phys. Rev. Lett.* **88** 67401
[19] Shah J 1999 *Ultrafast Spectroscopy of Semiconductors and Semiconductor Nanostructures* (Berlin: Springer)
[20] von der Linde D, Klingenberg H and Kuhl J 1980 *Phys. Rev. Lett.* **44** 1505
[21] Debye P 1914 *Ann. Phys., Lpz.* **43** 49
Waller I 1923 *Z. Phys.* **17** 398
see also Warren B E 1990 *X-ray Diffraction* (New York: Dover)
[22] Linac Coherent Light Source *LCLS Design-Report* http://www.ssrl.slac.stanford.edu/lcls/
[23] *TESLA XFEL Design-Report* http://xfel.desy.de
[24] Srinivasan R, Lobastov V A, Ruan Ch-Yu and Zewail A H 2003 *Helv. Chim. Acta* **86** 1763
[25] Siwick B J, Dwyer J R, Jordan R E and Miller R J D 2003 *Science* **320** 1382
Siwick B J, Dwyer J R, Jordan R E and Miller R J D 2004 *Chem. Phys.* **299** 285